Article

SOURCE DATA | TRANSPARENT PROCESS | OPEN ACCESS

EMBO reports

STING agonism turns human T cells into interferon-producing cells but impedes their functionality

Niklas Kuhl[1,2,†], Andreas Linder[1,2,*,†], Nora Philipp[1,3], Daniel Nixdorf[1,3], Hannah Fischer[1], Simon Veth[4], Gunnar Kuut[1], Teng Teng Xu[1,3], Sebastian Theurich[1,3,5,6], Thomas Carell[4], Marion Subklewe[1,3] & Veit Hornung[1]

Abstract

The cGAS-STING (cyclic GMP-AMP synthase-stimulator of interferon genes) axis is the predominant DNA sensing system in cells of the innate immune system. However, human T cells also express high levels of STING, while its role and physiological trigger remain largely unknown. Here, we show that the cGAS-STING pathway is indeed functional in human primary T cells. In the presence of a TCR-engaging signal, both cGAS and STING activation switches T cells into type I interferon-producing cells. However, T cell function is severely compromised following STING activation, as evidenced by increased cell death, decreased proliferation, and impaired metabolism. Interestingly, these different phenotypes bifurcate at the level of STING. While antiviral immunity and cell death require the transcription factor interferon regulatory factor 3 (IRF3), decreased proliferation is mediated by STING independently of IRF3. In summary, we demonstrate that human T cells possess a functional cGAS-STING signaling pathway that can contribute to antiviral immunity. However, regardless of its potential antiviral role, the activation of the cGAS-STING pathway negatively affects T cell function at multiple levels. Taken together, these results could help inform the future development of cGAS-STING-targeted immunotherapies.

Keywords antiviral immune response; cGAS; STING; T cell; T cell dysfunction
Subject Categories Immunology; Microbiology, Virology & Host Pathogen Interaction; Signal Transduction
DOI 10.15252/embr.202255536 | Received 3 June 2022 | Revised 5 January 2023 | Accepted 9 January 2023 | Published online 27 January 2023
EMBO Reports (2023) 24: e55536

Introduction

Pattern recognition receptors (PRRs) of the innate immune system recognize pathogen-associated molecular patterns (PAMPs) for antimicrobial defense. Activation of a PRR instills inflammation and elicits adaptive immune responses. Among these PRRs, cyclic GMP-AMP synthase (cGAS) specifically recognizes double-stranded DNA (dsDNA) inside the cell (Sun *et al*, 2013). Upon binding to dsDNA, cGAS produces cyclic GMP-AMP (cGAMP) (Ablasser *et al*, 2013; Diner *et al*, 2013; Gao *et al*, 2013; Zhang *et al*, 2013) that serves as a second messenger that binds to and thereby activates stimulator of interferon genes (STING) (Burdette *et al*, 2011). Activation of STING allows for the phosphorylation of interferon regulatory factor 3 (IRF3) by tank-binding kinase 1 (TBK1) (Ishikawa & Barber, 2008). Phosphorylated IRF3 relocates to the nucleus and drives the expression of antiviral genes, most notably type I interferons (type I IFN), such as IFNβ (Au *et al*, 1995; Lin *et al*, 1998). Type I IFNs stimulate the expression of antiviral interferon-stimulated genes (ISGs) in an autocrine and paracrine fashion by signaling through the interferon-α/β receptor (IFNAR). To a lesser extent, activation of STING also drives NF-κB pathway activation through an unresolved, noncanonical mechanism (Abe & Barber, 2014; Fang *et al*, 2017; de Oliveira Mann *et al*, 2019).

Apart from recognizing dsDNA introduced into the cytosol during infection with DNA viruses (Sun *et al*, 2013), recent studies additionally identified nuclear DNA during genotoxic stress (Dou *et al*, 2017; Glück *et al*, 2017; Harding *et al*, 2017; Mackenzie *et al*, 2017; Yang *et al*, 2017) and mitochondrial DNA (Rongvaux *et al*, 2014; White *et al*, 2014; West *et al*, 2015) during mitochondrial stress to activate cGAS-STING signaling. In light of these findings, cGAS has been linked to DNA damage sensing and might play a role

1 Gene Center and Department of Biochemistry, Ludwig-Maximilians-Universität München, Munich, Germany
2 Department of Medicine II, University Hospital, Ludwig-Maximilians-Universität München, Munich, Germany
3 Department of Medicine III, University Hospital, Ludwig-Maximilians-Universität München, Munich, Germany
4 Department of Chemistry and Center for NanoScience (CeNS), Ludwig-Maximilians-Universität München, Munich, Germany
5 German Cancer Consortium (DKTK), Partner site Munich, Heidelberg, Germany
6 German Cancer Research Center (DKFZ), Heidelberg, Germany
*Corresponding author. Tel: +49 (0)89 2180 71110; E-mail: hornung@genzentrum.lmu.de
†These authors contributed equally to this work

in the pathogenesis of autoimmune diseases, cellular senescence, and cancer (Li & Chen, 2018).

Although cGAS-STING signaling is commonly attributed to innate immune cells, there is increasing evidence that STING is also functional in adaptive immune cells, namely T cells. While STING activation can induce a type I IFN response from murine T cells (Larkin *et al*, 2017), it has also been reported that STING engagement impacts on T cell function beyond its antiviral role. *In vivo* studies employing the expression of a gain-of-function STING mutant observed severe T cell cytopenia and a greatly reduced memory T cell compartment (Cerboni *et al*, 2017; Warner *et al*, 2017; Bouis *et al*, 2019). However, there are conflicting views regarding the mechanism: Negative effects on T cell function were reported to occur independent of IRF3 or autocrine type I IFN signaling but rather attributed to a cell-intrinsic antiproliferative effect mediated by NF-kB (Cerboni *et al*, 2017) and cell death through ER stress (Wu *et al*, 2019a). Other studies suggest an IRF3-dependent upregulation of pro-apoptotic BH3-only proteins leading to cell death (Gulen *et al*, 2017) or IRF3/IRF7-dependent impairment of mTORC1, which was associated with reduced proliferation upon T cell receptor (TCR) stimulation, respectively (Imanishi *et al*, 2019).

In line with impaired T cell function observed in these studies, preclinical models suggest that STING-agonistic antitumor regimens are limited by the concomitant activation of the pathway within T cells (Sivick *et al*, 2018). Congruently, clinical phase I/II trials combining immunotherapy with STING agonists have seen mixed results in terms of efficacy (Le Naour *et al*, 2020). However, adoptive transfer of cGAS- or STING-deficient T cells has recently provided conflicting results in the murine system. T cell-intrinsic loss of the pathway impaired T cell functions when tumor antigen-specific T cells were transferred (Li *et al*, 2020) and STING activation enhanced antitumor responses through increased differentiation into effector cells (Benoit-Lizon *et al*, 2022). However, STING deficiency seemed to protect tumor-infiltrating T cells from cell death, when transferred T cells were allowed to endogenously mount an antitumor response (Wu *et al*, 2020). The reason for these discrepancies is unclear, but it is conceivable that the STING activation threshold plays a role in these different outcomes.

Since most of these observations stem from studying murine T cells and retrieved conflicting results, we here set out to better characterize outcomes of cell-intrinsic cGAS-STING signaling in primary human T cells by employing functional assays in combination with CRISPR/Cas9 gene editing. Doing so, we aimed to dissect IRF3-dependent from IRF3-independent functions mediated by STING and assess the role of auto- and paracrine type I IFNs.

Results

cGAMP induces antiviral cytokine release from T cell receptor-activated human T cells

To investigate whether the cGAS-STING pathway is operational in human T cells, primary CD4, and CD8 T cells isolated by magnetic bead separation (purity > 90%) were treated with the physiological STING agonist 2′-3′-cGAMP (cGAMP) (Fig 1A). In both cell types, cGAMP treatment alone induced the phosphorylation of STING (pSTING) and IRF3 (pIRF3). However, cGAMP-induced phosphorylation of STING and IRF3 was strongly enhanced if the cells were additionally activated through the engagement of their TCR and the provision of a co-stimulatory signal (αCD3/CD28 antibody-coated beads). Of note, αCD3/CD28 stimulation on its own failed to engage the STING-IRF3 axis in these cells. In line with the activation of IRF3, cGAMP also led to elevated levels of phosphorylated STAT1 (pSTAT1), which acts downstream of type I IFNs binding to the interferon-α/β receptor (IFNAR), indicating release and auto- or paracrine action of type I IFNs following cGAMP treatment. To assess whether T cell-intrinsic STING signaling could trigger the production of antiviral factors, IFNβ and the interferon-induced chemokine IP10 were measured in the supernatant of cGAMP stimulated T cells (Fig 1B and C). Of note, while cGAMP by itself was insufficient to elicit the production of measurable amounts of IFNβ and IP10, these antiviral factors became readily detectable in the supernatant of T cells co-treated with cGAMP and αCD3/CD28. Concentrations of IFNβ in the supernatant peaked at 16 h and remained detectable until 48 h, while the release of IP10 followed delayed kinetics, consistent with it being an interferon-stimulated gene (ISG). The release of IFNα, however, was quite heterogenous between donors with only one donor responding to αCD3/CD28/cGAMP co-treatment (Fig EV1A). To address whether the strong enhancement of STING and IRF3 phosphorylation observed in cGAMP- and αCD3/CD28-treated cells was due to auto- or paracrine effects, e.g., by TCR-dependent cytokines, we treated the cells with the translation inhibitor cycloheximide (CHX). These experiments, however, revealed that *de novo* protein synthesis was not required for this effect. CHX-treated cells showed the same enhancement of STING and IRF3 phosphorylation as untreated cells (Fig 1D), and the mRNA expression of IFNB and OASL remained unperturbed under these conditions (Fig 1E). Of note, CHX completely blunted the secretion of IFNγ that was seen in TCR-stimulated T cells (Fig EV1B). In line with these findings, using supernatant from αCD3/CD28-treated cells in conjunction with cGAMP stimulation was not able to substitute for the direct stimulation of T cells to trigger IFNβ expression (Fig EV1C). Further, to explore if STING activation in T cells is restricted to certain subsets (naïve, effector, memory), MACS-isolated naïve CD4 T cells were stimulated with cGAMP side by side with pan CD4 T cells from the same donor. Like the unsorted CD4 T cell population, naïve CD4 T cells also showed potent STING and IRF3 phosphorylation and IFNβ production when cGAMP and αCD3/CD28 beads were provided together (Fig EV1D and E). Taken together, these data show that primary human T cells display functional STING signaling upon exposure to cGAMP and that concomitant activation of the TCR greatly enhances signaling and is required for the release of antiviral cytokines. In addition, the synergy between STING and TCR stimulation is induced at a cell-intrinsic level.

Innate sensors cGAS and STING are operational in primary human T cells

Stimulator of interferon genes activation and subsequent type I IFN release induces the upregulation of interferon-stimulated genes (ISGs). Intrigued by the marked increase in STING signaling in human T cells through concomitant TCR activation, we set out to

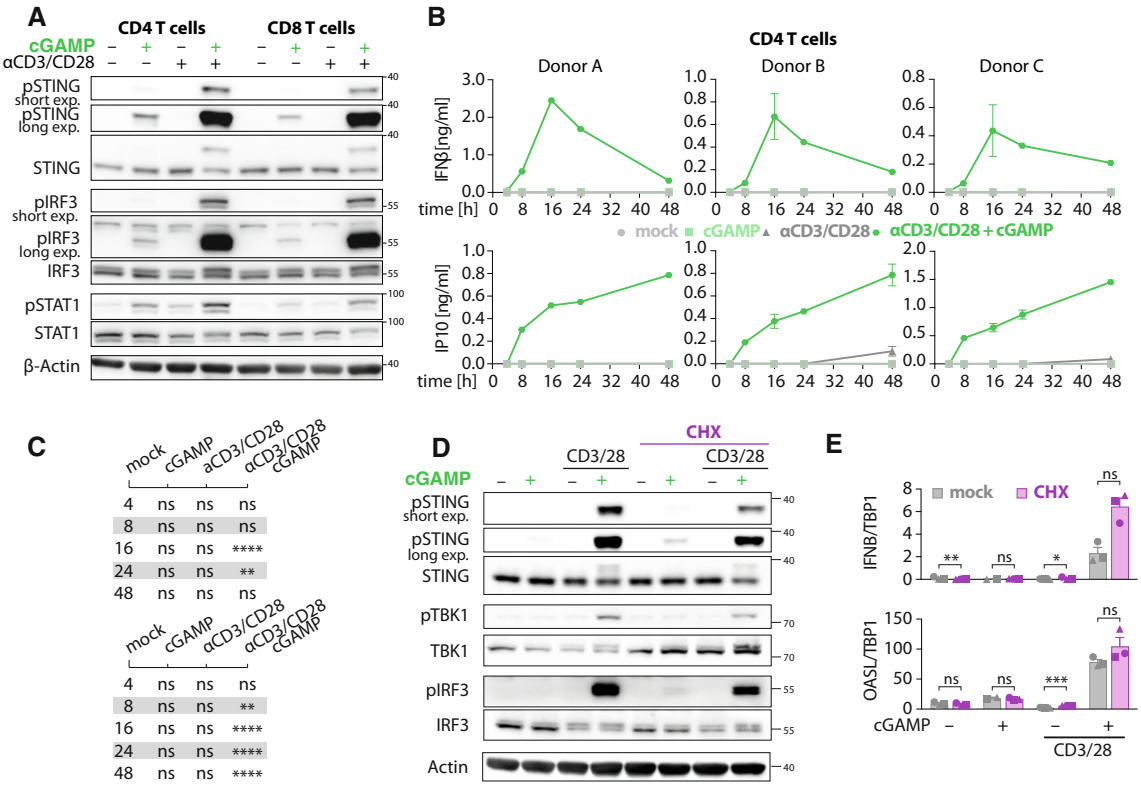

Figure 1. cGAMP treatment in addition to TCR stimulation leads to antiviral cytokine release in primary human T cells.

A CD4 and CD8 T cells were stimulated with cGAMP (20 μg/ml) and αCD3/CD28 beads as indicated. Cell lysates after 4 h of stimulation were analyzed by immunoblotting. Blots depict one representative donor out of three.

B CD4 T cells were stimulated with cGAMP (20 μg/ml) and αCD3/CD28; and human IFNβ (top) and IP10 levels (bottom) in the supernatant were analyzed by ELISA at the indicated time points. Data panels depict mean ± SD of biological duplicates from three independent donors.

C Statistics from (B) across all three donors indicate significance by a repeated-measures two-way ANOVA with Dunnett correction for multiple testing: ****$P < 0.0001$; **$P < 0.01$; ns, not significant.

D CD4 T cells were left untreated or pretreated with cycloheximide (2 μg/ml) for 2 h, then treated with cGAMP (20 μg/ml) and αCD3/CD28 (3/28) for 4 h. Lysates were analyzed by immunoblotting. One representative donor out of two is shown.

E CD4 T cells were left untreated or pretreated with cycloheximide (2 μg/ml) for 2 h, then treated with cGAMP (20 μg/ml) and αCD3/CD28 (3/28) for 4 h, then analyzed by quantitative PCR for *IFNB1* and *OASL* expression. Data are depicted as mean + SEM of three independent donors (for cGAMP treated cells without CHX only two data points were obtained). Statistics were determined by a two-way ANOVA on log-transformed data using Šidák correction for multiple testing: ***$P < 0.001$; **$P < 0.01$; *$P < 0.05$; ns, not significant.

Source data are available online for this figure.

characterize this phenotype more thoroughly by employing an unbiased approach. To this end, the same conditions as in the previous experiment were employed: T cells were either left untreated or stimulated with cGAMP and additionally stimulated using αCD3/CD28 beads or not (Fig EV2A). To account for potential impurities in our T cell preparations and STING-independent effects of cGAMP, these experiments were conducted in CD4 T cell clones that were either wildtype (WT) or in which the STING locus was disrupted by CRISPR/Cas9 gene editing (*STING1*$^{-/-}$). Pooled clones were stimulated for 4 h in triplicates and then subjected to RNA-Seq analysis. Principal component analysis (PCA) retrieved four distinct groups representing the four experimental conditions of the WT clones (Fig 2A): unstimulated cells (gray), cGAMP treatment (green), αCD3/CD28 treatment (purple), and αCD3/CD28 + cGAMP co-treatment (blue). Clustering of these groups was confirmed by *k*-means clustering (Fig EV2B). Of note, cGAMP-treated *STING1*$^{-/-}$ clones clustered with unstimulated WT cells, while *STING1*$^{-/-}$ cells co-treated with αCD3/CD28 and cGAMP clustered with WT cells stimulated with αCD3/CD28 only. These observations support the notion that there are no STING-independent effects of cGAMP in human T cells. Apart from that, WT and *STING1*$^{-/-}$ T cells showed minor differences in gene expression under steady-state conditions (Fig EV2C) or following αCD3/CD28 treatment (Fig EV2D). To this end, a few ISGs were expressed in WT, but not in *STING1*$^{-/-}$ cells, suggesting a steady-state activity of the STING pathway in the absence of exogenous triggers. Focusing on transcripts associated with a type I IFN response among the most variable genes (Fig EV2E) showed a strong ISG induction following STING activation in T cells: cGAMP treatment led to a STING-dependent upregulation of classical ISGs, whose expression was enhanced when co-treating with αCD3/CD28 (Fig 2B). This was corroborated by comparing the main clusters retrieved in the PCA to identify

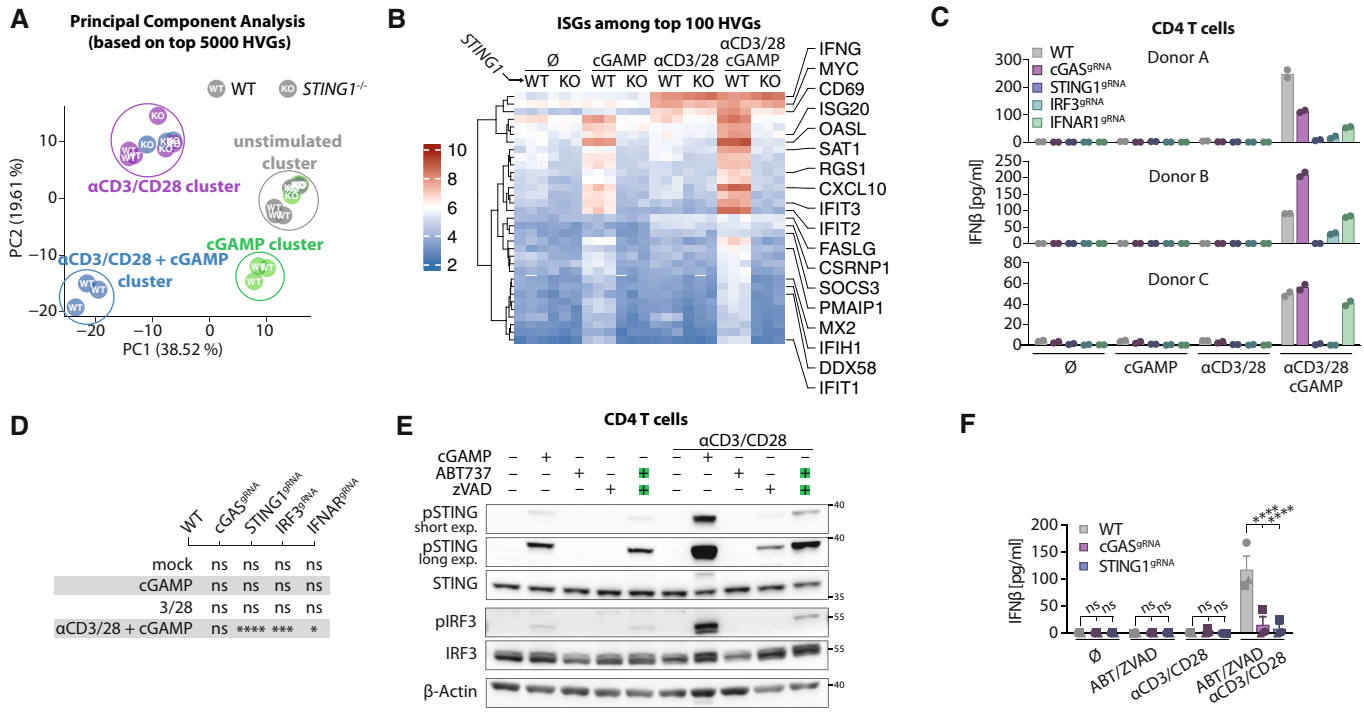

Figure 2. Primary human T cells display canonical STING signaling.

A Pooled CD4 T cell WT and *STING1*$^{-/-}$ clones were stimulated in triplicates with cGAMP (20 μg/ml) and αCD3/CD28 for 4 h and analyzed by RNA sequencing. Principal component analysis based on the top 5,000 highly variable genes (HVGs).

B Heatmap showing interferon-stimulated genes (ISGs) among the top 100 HVGs according to (Samarajiwa *et al*, 2009) clustered hierarchically across all conditions and replicates. Color coding corresponds to normalized and log2-transformed read counts. Genes differentially expressed between cGAMP-treated and cGAMP + αCD3/CD28-treated conditions are annotated.

C CRISPR/Cas9 targeted CD4 T cells for indicated genes were treated with cGAMP (20 μg/ml) and αCD3/CD28 beads for 48 h. Human IFNβ levels were analyzed by ELISA. Data panels depict the mean of biological duplicates from three independent donors.

D Statistics from (C) across all three donors indicate significance by a repeated-measures two-way ANOVA with Dunnett correction for multiple testing: ****$P < 0.0001$; ***$P < 0.001$; *$P < 0.05$; ns, not significant.

E CD4 T cells were stimulated with the indicated stimuli for 4 h. Lysates were analyzed by immunoblotting. One representative donor out of three is shown.

F CRISPR/Cas9 targeted CD4 T cells for the indicated genes were treated with the indicated stimuli for 48 h. Human IFNβ levels were analyzed by ELISA. Data are depicted as mean + SEM of three independent donors. Statistics indicate significance by two-way ANOVA with Dunnett correction for multiple testing: ****$P < 0.0001$; ns, not significant.

Source data are available online for this figure.

differentially expressed genes: While cGAMP treatment alone could already induce expression of several ISGs (e.g., *IFIT2*, *IFIT3*, *OASL*, *IFIT1*) (Fig EV2F), treatment with αCD3/CD28 mostly induced genes associated with TCR stimulation and NF-κB signaling (e.g., *TNF*, *CD69*, *NFKBID*, *IFNG*) (Fig EV2G). Of note, many ISGs were among those genes differentially expressed between cGAMP-treated cells and cGAMP + αCD3/CD28-treated cells; verifying that co-treatment with αCD3/CD28 enhances ISG expression (Fig EV2H). Altogether, these data implicated that STING activation in human T cells leads to an antiviral transcriptional program that is enhanced and diversified by concomitant TCR stimulation.

To validate if cGAS-STING signaling in human T cells employs canonical components of signal transduction, we generated polyclonally CRISPR/Cas9-edited CD4 T cells targeting *CGAS*, *STING1*, *IRF3*, and *IFNAR1*. Analyzing levels of the respective proteins by immunoblotting revealed a substantial loss of expression from the targeted locus (Fig EV3A). Successful disruption of IFNAR-signaling in *IFNAR1* targeted cells was confirmed by exposing T cells to IFNα2a, which revealed decreased STAT1 phosphorylation in cells nucleofected with gRNAs directed against *IFNAR1* but not other targets. T cells obtained by this approach were then treated with cGAMP with or without αCD3/CD28 co-treatment and analyzed for IFNβ levels in the supernatant (Fig 2C and D). As expected, co-treatment with cGAMP and αCD3/CD28 resulted in IFNβ release from WT and cGAS-deficient cells. Yet, IFNβ release was entirely dependent on STING and IRF3, suggesting canonical signaling downstream of STING activation in T cells. IFNβ release was also partially dependent on IFNAR1, suggesting an enhancement of IFNβ production through a positive feedback loop. To evaluate the contribution of autocrine type I IFNs, *IFNAR1* deficient cells were analyzed for IFNβ and IP10 secretion in a time course experiment. As polyclonal gene targeting of *IFNAR1* still led to residual STAT1 phosphorylation upon exposure to IFNα (Fig EV3A), clonal *IFNAR1*-deficient T cells were employed for this experiment. STING activation by cGAMP and αCD3/CD28 treatment led to initial IFNAR1-independent IFNβ release after 8 h. Consecutive IFNβ secretion,

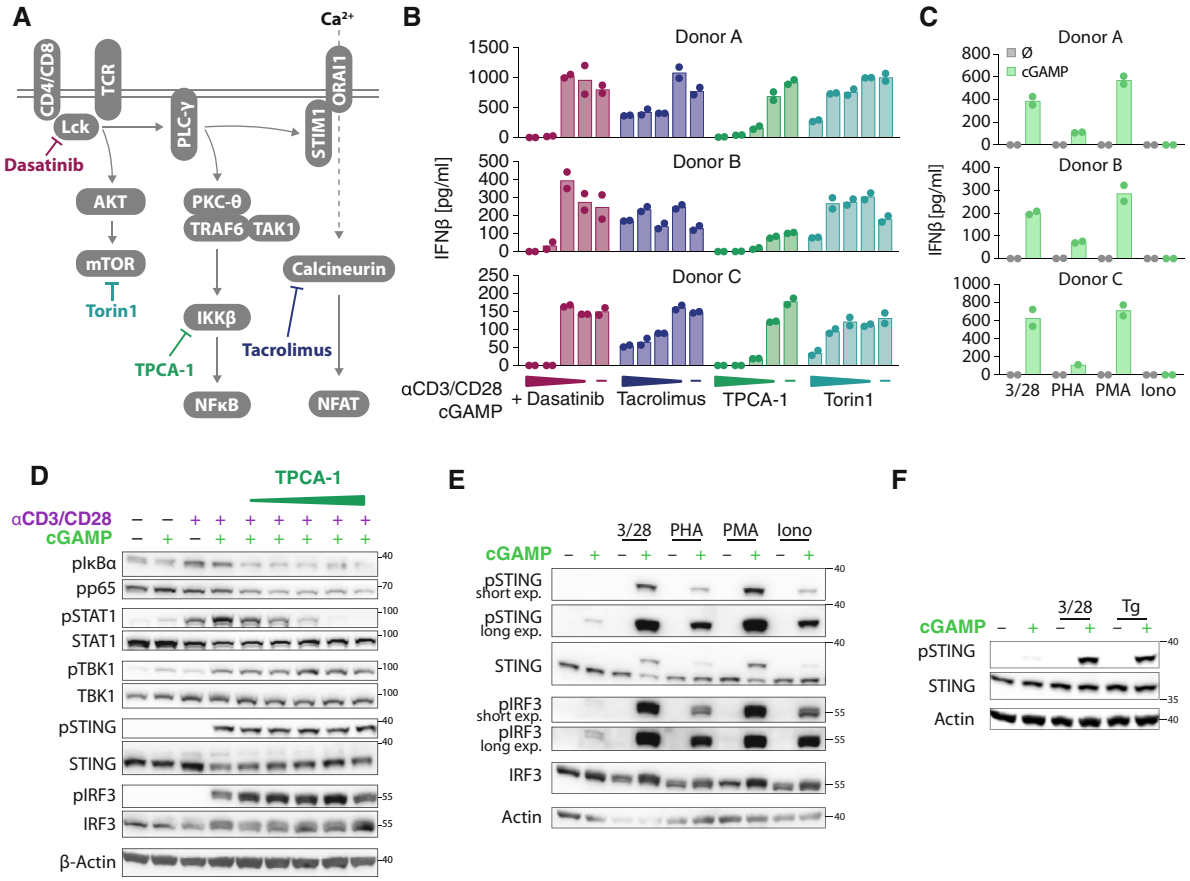

Figure 3. Critical role for NF-kB signaling in STING-driven antiviral immunity.

A Simplified model of signaling downstream of TCR engagement.

B CD4 T cells were pretreated with Dasatinib (100, 10, 1 and 0.1 nM), Tacrolimus (1,000, 100, 10 and 1 nM), TPCA-1 (4, 2, 1 and 0.5 μM), and Torin1 (50, 5, 0.5 and 0.05 nM) for 30 min, then treated with cGAMP (20 μg/ml) and αCD3/CD28 for 16 h. Human IFNβ levels in the supernatant were analyzed by ELISA. Data panels depict the mean of biological duplicates from three independent donors.

C CD4 T cells were treated with cGAMP (20 μg/ml) and indicated additional stimuli for 16 h. Human IFNβ levels were analyzed by ELISA. Data panels depict the mean of biological duplicates from three independent donors (for cGAMP and PHA-treated cells of Donor C only one data point was obtained).

D CD4 T cells were treated with cGAMP and indicated stimuli together with increasing concentrations of TPCA-1 for 4 h. Cell lysates were analyzed by immunoblotting. One representative donor out of two is shown.

E, F CD4 T cells were stimulated with cGAMP (20 μg/ml) and additional stimuli as indicated. Cell lysates after 4 h of stimulation were analyzed by immunoblotting. One representative donor out of two is shown.

Source data are available online for this figure.

however, was mostly dependent on IFNAR1 (Fig EV3B), again suggesting that a positive feedback loop was operable. IP10 release was completely dependent on IFNAR1 throughout the whole time course (Fig EV3C), indicating that autocrine type I IFN signaling is critical to reinforce antiviral cytokine production upon STING activation in human T cells. In summary, IFNβ release from human T cells upon STING activation is facilitated through IRF3 and relies on a feedback loop dependent on the type I IFN receptor IFNAR for full-scale activation.

Having established that STING is operational in human T cells, we set out to explore whether cGAS binding to double-stranded DNA can activate STING in human T cells and if this results in downstream type I IFN production. While transfecting dsDNA readily induced STING phosphorylation in peripheral blood mononuclear cells (PBMCs), it failed to do so in purified primary human T cells (Fig EV3D). To account for the possibility that exogenous dsDNA was not active due to insufficient delivery, we investigated if cGAS could get activated by endogenous DNA. To this end, previous work has established that DNA released in the context of mitochondrial outer membrane permeabilization (MOMP) can engage the cGAS-STING axis, if concomitant induction of intrinsic apoptosis is prevented (Rongvaux *et al*, 2014; White *et al*, 2014). To test this scenario, we treated T cells with the Bcl2-inhibiting drug ABT737, which results in the release of mtDNA into the cytosol. To prevent the cells from undergoing apoptosis that is known to otherwise interfere with cGAS activation (Ning *et al*, 2019), cells were additionally treated with the pan-caspase inhibitor zVAD. Treating human T cells with the combination of these tool compounds led to phosphorylated STING and IRF3; similar to cells treated with cGAMP (Fig 2E). Again, αCD3/CD28 co-treatment amplified STING

signaling, however, not to the same extent as cGAMP activity was amplified by αCD3/CD28. To genetically validate that the induction of type I IFNs through this treatment is a result of cGAS activation, we employed polyclonal CRISPR/Cas9 gene editing and generated CD4 T cells deficient for either cGAS or STING. Treating these cells with ABT737 and zVAD led to IFNβ release that was completely dependent on cGAS and STING, while IFNγ levels were unchanged between genotypes (Figs 2F and EV3E). In conclusion, these data support that not only STING but also the PRR cGAS is functional and can be activated by MOMP-derived mtDNA in human T cells.

TCR engagement boosts IFNβ production via at least two independent mechanisms

Based on the observation that TCR stimulation is a prerequisite for IFNβ release from human T cells, we set out to explore what signaling events downstream of TCR signaling are required for the production of IFNβ. To do so, we employed a series of small molecule inhibitory compounds acting downstream of the TCR (Fig 3A). As expected, inhibition of apical signal transduction downstream of TCR stimulation by targeting Lck with the tyrosine kinase inhibitor Dasatinib completely abrogated the IFNβ response (Fig 3B). On the other hand, the calcineurin-inhibitor Tacrolimus failed to substantially block IFNβ release at concentrations well above those needed to block NFAT activity (Dufva *et al*, 2020), excluding a role for this transcription factor in IFNβ production. However, employing TPCA-1 to block IKKβ, the critical kinase of the NF-kB activating IKK complex, potently blunted IFNβ release. Since recent findings suggested that type I IFN production is regulated by mTORC1 (Imanishi *et al*, 2019) we also employed the mTOR inhibitor Torin1. Indeed, the inhibition of mTOR reduced IFNβ release from CD4 T cells, although to a lesser extent than TPCA1. Both TPCA-1 and Torin1 inhibited the antiviral response at the level of mRNA expression, excluding a role for post-transcriptional regulation (Fig EV3F). In line with a critical role for NF-kB activation in the IFNβ response of T cells, stimuli converging on NF-κB activation, such as phorbol myristate acetate (PMA) and to a lesser extent Phytohaemagglutinin (PHA) could also substitute the anti-CD3/CD28 signal to induce IFNβ secretion in conjunction with cGAMP (Fig 3C). Conversely, the Ca^{2+} ionophore Ionomycin together with cGAMP was not able to trigger IFNβ production. Altogether, these results suggested that TCR-dependent NF-κB activation might be a critical signal required to facilitate IFNβ expression, which is well in line with the notion that the IFNβ promoter harbors NF-κB binding sites that need to be engaged to drive its expression (Iwanaszko & Kimmel, 2015). Immunoblotting confirmed impaired NF-κB signaling through TPCA-1 as evidenced by decreased levels of IκBα phosphorylation (Fig 3D). Moreover, in line with the inhibition of IFNβ production, TPCA-1 treatment abrogated paracrine and autocrine type I IFN activity as evidenced by a reduced STAT1 phosphorylation. Interestingly, TPCA-1 treatment had no impact on the phosphorylation levels of TBK1, STING, and IRF3, which suggested that TCR signaling generates at least one additional signal that boosts cGAMP-dependent antiviral activity. We noted that the Ca^{2+} ionophore Ionomycin, which failed to synergize with cGAMP to induce IFNβ production (Fig 3C), was able to trigger potent STING and IRF3 phosphorylation when added together with cGAMP (Fig 3E). These results suggested that Ca^{2+} flux could provide the signal required for synergistic STING activation. Along these lines, the treatment of cells with Thapsigargin, which increases cytosolic Ca^{2+} levels but decreases ER-Ca^{2+} levels by inhibiting ER-Ca^{2+}-ATPases, also acted synergistically with cGAMP in inducing strong STING phosphorylation (Fig 3F). In summary, these results suggest that T cell receptor engagement facilitates STING signaling at least two independent steps: On the one hand, TCR-dependent NF-kB activation is critically required to drive IFNβ expression, presumably directly at the level of the *IFNB* promoter. On the other hand, TCR-dependent Ca^{2+} flux appears to boost STING activation as early as at the level of STING phosphorylation.

STING activation induces IRF3-dependent apoptosis in primary human T cells

Unexpectedly, treating CD4 T cells with increasing concentrations of cGAMP did not translate into an increase in IFNβ production but rather a drastic decrease (Fig EV4A). Monitoring cell viability revealed that the decrease in IFNβ production was accompanied by a lower number of viable cells at high cGAMP concentrations (Fig EV4B). In light of these results and previous reports in that regard (Gulen *et al*, 2017; Larkin *et al*, 2017; Wu *et al*, 2019a), which suggested a pro-apoptotic function of STING, we further characterized cell death by staining for Annexin V, a marker for early apoptosis. Treating CD4 T cells with increasing concentrations of cGAMP resulted in increased cell death (Fig 4A), while this was not prevented by αCD3/CD28 co-treatment. Of note, slightly increased levels of cell death as observed in the αCD3/CD28 treated conditions can be attributed to the phenomenon of activation-induced cell death (AICD) (Green *et al*, 2003). As a control, we treated cells with a combination of the Bcl2-inhibitor ABT737 and the Mcl1-inhibitor S63845, which is known to robustly induce intrinsic apoptosis in human T cells (Linder *et al*, 2020). Studying the response of freshly isolated CD4 and CD8 T cells revealed that both T cell types undergo cell death upon cGAMP treatment (Fig 4B). CD8 T cells, however, appear to be more susceptible to AICD, resulting in a higher overall number of dead cells in the αCD3/CD28 co-treated conditions. Both cell types responded to ABT737/S63845-induced cell death as expected. To better understand the mode of cell death elicited by cGAMP treatment, we reevaluated our RNA-Seq dataset for differentially expressed genes under the GO term "Positive regulation of apoptotic process" (Fig EV4C). cGAMP treatment of CD4 T cells led to STING-dependent upregulation of several transcripts associated with apoptosis, including the anti-apoptotic *MCL1* and pro-apoptotic *PMAIP1* (coding for Noxa) genes, which have been well studied in this context. Other genes linked to apoptosis like *IFNG*, *FASLG*, and *RGCC* were associated with TCR stimulation rather than STING activation, because they were induced independently of cGAMP and STING in the presence of αCD3/CD28 treatment. In line with apoptosis being the main type of cell death triggered by STING activation in T cells, increasing concentrations of cGAMP led to caspase 3 and PARP cleavage like ABT737/S63845 treatment (Fig 4C). Employing polyclonal CRISPR/Cas9 gene editing revealed that STING- and IRF3-deficient T cells were completely protected from cGAMP-induced cell death, while cGAS and IFNAR1-deficiency had no effect (Fig 4D and E). As expected, intrinsic apoptosis by ABT737/S63845 occurred independently of these gene deficiencies. This again suggested that STING triggers an interferon-independent, cell-intrinsic

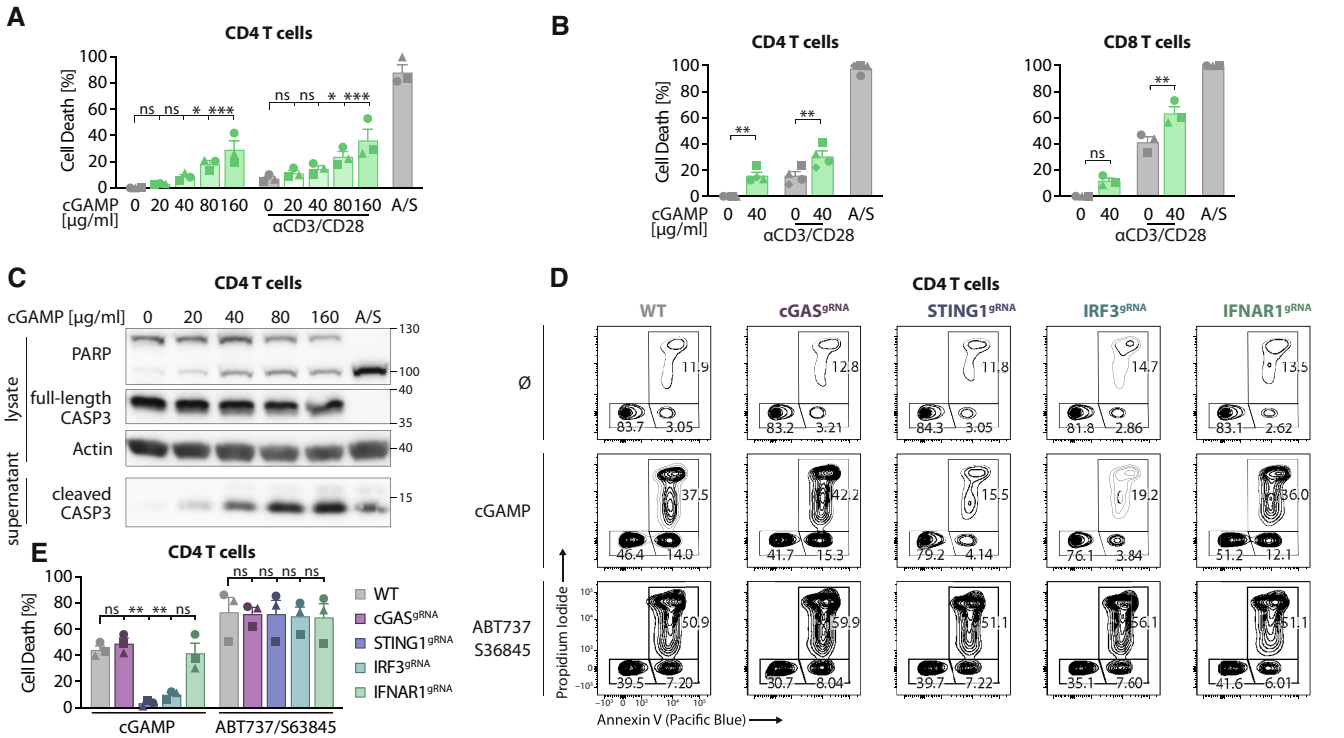

Figure 4. STING activation induces cell death in primary human T cells.

A Freshly isolated CD4 T cells were treated with cGAMP, αCD3/CD28 beads, and ABT737/S63845 (A/S) for 48 h and analyzed by flow cytometry. Treatment-induced cell death was assessed by Annexin V and propidium iodide staining. Data are depicted as mean + SEM of three independent donors. Statistics indicate significance by two-way ANOVA with Dunnett correction for multiple testing: ***$P < 0.001$; *$P < 0.05$; ns, not significant.

B Freshly isolated CD4 (left) and CD8 (right) T cells were treated as indicated for 48 h and analyzed by flow cytometry. Treatment-induced cell death was assessed by Annexin V and propidium iodide staining. Data are depicted as mean + SEM of 4 (CD4) or 3 (CD8) independent donors. Statistics indicate significance by two-way ANOVA with Šidák correction for multiple testing: **$P < 0.01$; ns, not significant.

C CD4 T cells were treated with indicated concentrations of cGAMP for 18 h, and ABT737/S63845 for 2 h. Lysates and supernatant precipitations were analyzed by immunoblotting. One representative donor out of two is shown.

D CRISPR/Cas9 targeted CD4 T cells for indicated genes were treated with the indicated stimuli for 48 h and analyzed by flow cytometry. Each panel shows propidium iodide and Annexin V intensity for one representative donor out of three. Digits indicate the percentage of the parental population (single events without subcellular debris).

E Summary from (D), whereas data are depicted as mean + SEM of three independent donors. Statistics indicate significance by two-way ANOVA with Dunnett correction for multiple testing: **$P < 0.01$; ns, not significant.

Source data are available online for this figure.

mechanism, where IRF3 most likely mediates transcriptional changes leading to apoptosis. In summary, these results suggested that STING activation in T cells induces apoptotic cell death in human T cells fully dependent on IRF3.

STING activation impairs proliferation in primary human T cells independent of IRF3 and autocrine type I IFN

Studies employing T cells ectopically overexpressing a patient-derived gain-of-function STING mutant suggested an antiproliferative effect of STING on TCR-stimulated T cells (Cerboni *et al*, 2017). To evaluate whether STING activation via cGAMP influences the proliferation of TCR-stimulated human T cells, CellTrace Violet (CTV) dilution was determined by flow cytometry (Fig 5A). When CD4 and CD8 T cells were kept resting, cells did not divide, indicated by a single brightly stained peak (light gray profile). When activated with αCD3/CD28, T cells proliferated readily resulting in a profile with several peaks representing cell division events (black profile). However, when additionally adding cGAMP to the cells on day 0 and day 2, T cell proliferation was markedly reduced (green profile). Quantification by proliferation modeling to compare results across several different donors showed that cGAMP has a substantial negative effect on T cell proliferation after activation of both CD4 and CD8 T cells (Fig 5B). Analyzing the proliferation of CD4 T cells deficient for *CGAS*, *STING1*, *IRF3*, and *IFNAR1* generated by CRISPR/Cas9 gene editing revealed that wildtype and *CGAS*-deficient T cells proliferated less when treated with cGAMP, while cGAMP-treated *STING1*-deficient T cells behaved like the αCD3/CD28 treated control condition (Fig 5C). Interestingly, *IRF3*- and *IFNAR1*-deficient cells were not protected from impaired proliferation, suggesting an IRF3-independent, cell-intrinsic mechanism rather than an effect of para/autocrine type I IFNs or IRF3-dependent transcription itself (Fig 5D). Upon TCR-mediated activation, T cells engage both

mitochondrial oxidative phosphorylation (OXPHOS) and glycolysis to meet the energy demands required for proliferation and effector functions. To investigate cGAMP-mediated alterations in the basal and maximal metabolic capacity of T cells during αCD3/CD28 activation, we next performed metabolic stress tests. Following CD3/CD28 engagement, T cells strongly increased both their respiratory capacity and their glycolytic rate. Increased mitochondrial respiration mediated by αCD3/CD28 activation was substantially reduced when T cells were additionally treated with cGAMP while resting T cells only displayed marginal changes in respiratory capacity (Fig 5E). cGAMP treatment reduced basal respiration in activated T cells, suggesting less energetic demand in baseline conditions. Moreover, maximal respiration after mimicking maximal energetic demands and the reserve capacity was substantially reduced, impacting the cells' ability to respond to metabolic challenges adequately. In addition, high basal glycolysis after glucose injection upon CD3/CD28 activation was substantially reduced when T cells were activated in the presence of cGAMP (Fig 5F). Similar to oxidative phosphorylation, basal glycolysis, maximal glycolytic capacity, and the glycolytic reserve were impaired by cGAMP treatment, indicating reduced glycolysis in baseline and anaerobic conditions, as well as a reduced capacity to respond to energetic demands. Overall, these data suggested that STING activation impairs activation-induced proliferation in human T cells in a process for which IRF3 and type I IFNs are dispensable. Moreover, STING activation compromises metabolic functions necessary for T cell proliferation.

Discussion

While extensively studied in cells of the innate immune system, fibroblasts and epithelial cells, more recent data suggest that the cGAS-STING pathway is also operational in T cells. As these data with few exceptions rely on the study of murine T cells, we here provide a detailed characterization of the cGAS-STING pathway in primary human CD4 and CD8 T cells. Employing the physiological STING ligand 2′-3′-cGAMP revealed that human T cells do not only express high levels of STING but retain functional signaling evidenced by phosphorylation of STING, IRF3, as well as secretion of considerable amounts of IFNβ and the interferon-stimulated chemokine IP10. Interestingly, and similar to the mouse system (Imanishi

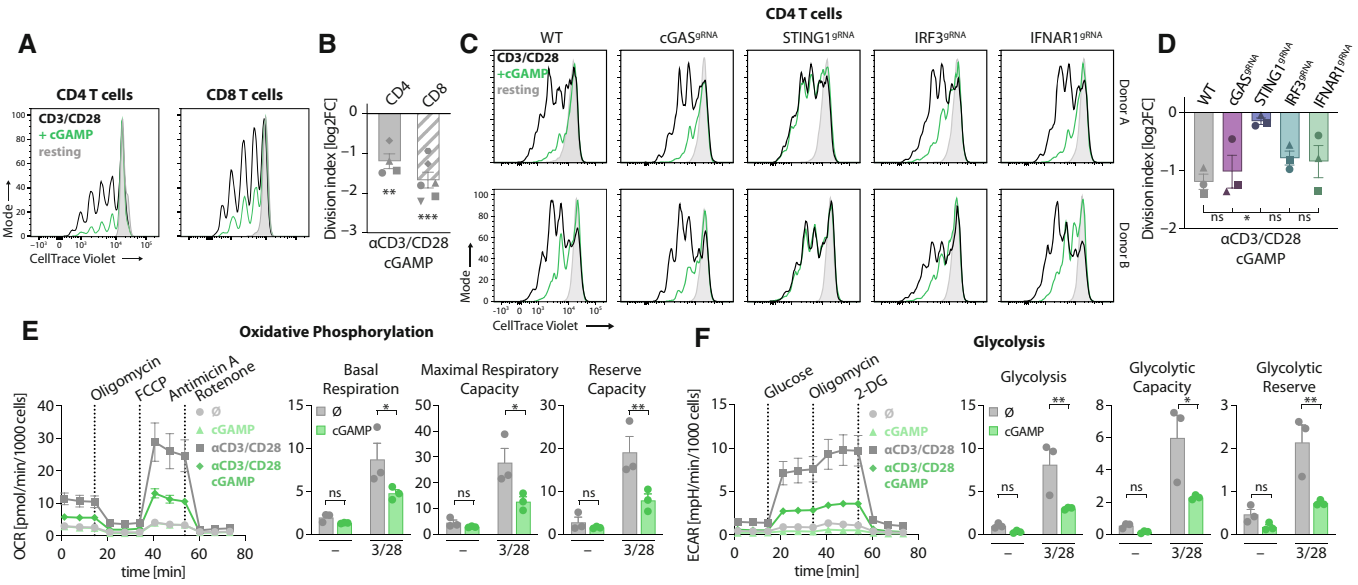

Figure 5. STING activation impairs proliferation in primary human T cells.

A CellTrace Violet (CTV) stained, freshly isolated CD4 and CD8 T cells were activated with αCD3/CD28 beads, stimulated with cGAMP for 96 h, and analyzed by flow cytometry. Each panel shows profiles from activated (black), cGAMP-treated (green), and resting (light gray) single and live cells from one representative donor.

B Summary from (A) across four (CD4) or six (CD8) independent donors. Division indices for each condition were calculated using proliferation modeling. Plot shows log2-transformed fold changes (log2FC) of division indices of treated samples compared to those of activated samples without any additional treatment. Individual data points ± SEM are shown. Statistics indicate significance by one-sample *t*-test: ***$P < 0.001$; **$P < 0.01$.

C CRISPR/Cas9 targeted CD4 T cells for indicated genes were treated with cGAMP for 96 h, analyzed by flow cytometry, and subjected to the same analysis as in (A). Two representative donors out of three are shown.

D Summary of (C) across three independent donors, analyzed as in (B). Data are depicted as mean ± SEM of three independent donors. Statistics indicate significance by one-way ANOVA with Dunnett correction for multiple testing: *$P < 0.05$; ns, not significant.

E Freshly isolated CD4 T cells were treated with cGAMP (40 μg/ml) and αCD3/CD28 (3/28) for 48 h and analyzed by Seahorse XF Mito Stress Test. Data are depicted as mean ± SEM of three independent donors. Statistics indicate significance by two-way ANOVA with Šidák correction for multiple testing: **$P < 0.01$; *$P < 0.05$; ns, not significant.

F Cells treated as in (E) were subjected to the Seahorse XF glycolysis stress test. Data are depicted as mean ± SEM of three independent donors. Statistics indicate significance by two-way ANOVA with Šidák correction for multiple testing: **$P < 0.01$; *$P < 0.05$; ns, not significant.

Source data are available online for this figure.

et al, 2019), simultaneous TCR activation was required for a potent antiviral response in T cells. TCR engagement provides at least two independent signals to boost STING signaling. On the one hand, TCR-dependent IKK activation provides the critical NF-κB activity that is necessary for efficient *IFNB1* expression together with STING-dependent IRF3 phosphorylation. On the other hand, TCR signaling is also required for efficient activation of the STING axis in the first place, as evidenced by phosphorylation of TBK1, STING, and IRF3. Here, it appears that signals that deplete ER Ca^{2+} stores potently boost STING activation, presumably by facilitating its exit from the ER. By genetically disrupting the expression of cGAS, STING, IRF3, and IFNAR1 in primary human T cells we confirm that STING signaling relies on IRF3 for cytokine production. In addition, an autocrine feedback loop reinforces type I IFN production and facilitates the induction of ISGs. While we failed to induce cGAS-dependent STING-activation through cytoplasmic delivery of exogenous immunostimulatory DNA, we readily could detect STING-activation upon MOMP-induction when caspases are inhibited pharmacologically in parallel (Rongvaux *et al*, 2014; White *et al*, 2014). Genetically, this relied on cGAS, proving that also cGAS is functional in human T cells. In addition to cytokine secretion, T cell-intrinsic STING activation induces cell death that displays features of apoptosis and in human cells genetically depends on IRF3 but is unlike cytokine secretion independent of concomitant TCR activation and autocrine IFNAR1-signaling. Upon exposure to cGAMP, T cell proliferation is heavily impaired, similar to what has been observed when *gain-of-function* STING variants were overexpressed in human T cells (Cerboni *et al*, 2017). Unlike cell death and cytokine production, the brake that STING activation puts on proliferation is independent of IRF3. Finally, we observe that also the metabolic changes associated with TCR engagement are corrupted in the presence of a STING agonist, supporting that various T cell functions are impaired when STING is activated in this cell type.

Requirement for TCR activation for STING-dependent type I IFN production

While resting CD4 and CD8 T cells were capable of canonical STING pathway activation, subsequent type I IFN production required simultaneous TCR stimulation. Based on our results, we propose at least two independent pathways to be operational:

First, using the IKKβ inhibitor TPCA-1, we found that blocking NF-κB signaling effectively abrogated type I IFN production but had no effect on STING or IRF3 phosphorylation, suggesting that TCR stimulation provides NF-κB signaling required for type I IFN production. This is in line with the notion that NF-κB acts as a critical transcription factor for *IFNB1* gene expression (Honda *et al*, 2006). Yet, unlike in other cell types, NF-κB activation downstream of STING activation appears to be insufficient for the induction of type I IFN in T cells. Our findings also confirm that TCR-dependent mTORC1 activation is required for IFNβ production, which was recently suggested for murine T cells (Imanishi *et al*, 2019). mTORC1 is a protein complex being assembled after T cell activation and linked to metabolic reprogramming and increased protein translation during T cell proliferation. As mTORC1 is also involved in NF-κB activation following TCR engagement, it remains unclear from these data if mTORC1 enhances IFNβ production through NF-κB or through a different mechanism. In fact, Imanishi *et al* (2019) show that mTORC1 inhibition reduces protein levels of IRF7, another transcription factor involved in type I IFN signaling.

Second, only the combination of CD3/CD28 stimulation and cGAMP treatment resulted in strong phosphorylation of TBK1, STING, and IRF3, which occurred independently of IKK activation. Our data suggest that TCR-dependent Ca^{2+} signaling is required for this activity. To this end, either Ionomycin, which acts as a Ca^{2+} ionophore at the plasma and ER membranes, or Thapsigargin, which depletes ER Ca^{2+} levels by inhibiting the ER Ca^{2+}-ATPase, were able to potently boost STING and IRF3 phosphorylation together with cGAMP. We hypothesize that these compounds facilitate STING activation via engaging the ER-Ca^{2+} sensor STIM1. When Ca^{2+} levels drop in the ER, STIM1 oligomerizes and subsequently translocates to the plasma membrane to activate Ca^{2+}-selective Orai channels (Soboloff *et al*, 2012). However, recent work has shown that ER-resident STIM1 also exerts a negative regulatory function on STING by restraining it in the ER. As such, the deletion of STIM1 results in the spontaneous, ligand-independent translocation of STING from the ER, resulting in its activation (Srikanth *et al*, 2019). We speculate that the lowering of ER Ca^{2+} stores, as it physiologically occurs upon TCR engagement, and as it is synthetically triggered by Ionomycin and Thapsigargin, facilitates the STIM1-dependent exit of STING from the ER to gain its signaling competent state. However, additional mechanistic studies are required to corroborate this assumption.

Mechanisms of STING-mediated effects beyond IFN production

Stimulator of interferon genes activation led to apoptosis in human T cells. We identified IRF3 as the key mediator of this cell death program, as the deletion of IRF3 completely abrogated STING-induced cell death. In fact, previous research in murine T cells reported IRF3-dependent upregulation of the pro-apoptotic BH3-only protein Noxa (*PMAIP1*) resulting in apoptotic cell death (Gulen *et al*, 2017). However, in the same study, STING activation was also found to trigger—via a yet to be defined mechanism—a p53-dependent signaling pathway that cooperates with IRF3 in the induction of pro-apoptotic genes. Specifically, the BH3-only protein Puma was shown to be highly induced in murine T cells by a p53-dependent but IRF3-independent mechanism following STING activation. Consistent with a dual requirement of IRF3- and p53-dependent mechanisms downstream of STING, murine T cells were only partially rescued from STING-dependent cell death when either transcription factor was absent. However, the fact that human IRF3-deficient T cells become fully resistant to cell death upon STING activation does not support the existence of a p53-dependent pathway in human T cells. Indeed, while we detected upregulation of the well-known ISG Noxa (*PMAIP1*) through RNA-Seq, we failed to observe cGAMP-mediated upregulation of Puma. Aside from promoting pro-apoptotic gene expression, IRF3 was also shown to directly interact with Bax, a protein of the pro-apoptotic Bcl2 family, through a BH3 domain initiating the mitochondrial apoptotic pathway (Chattopadhyay *et al*, 2010). Strikingly, the function of IRF3 as a transcriptional regulator is not necessary for the interaction with Bax, suggesting multiple death-inducing functions for activated IRF3. Noteworthy, our findings also imply that IRF3-independent modes of cell death via ER stress after STING activation as previously reported in murine T cells expressing SAVI-mutant STING (Wu *et al*, 2019a) only play a

negligible role in human T cells. However, as our model involves acute activation using the physiological agonist cGAMP these findings might not apply to T cells that chronically activate STING through a gain-of-function mutation. Worth mentioning, if GOF mutations also display synergistic activation following TCR stimulation, T cell activation during infection could exacerbate symptoms in patients carrying such mutations.

Besides cell death, we also observed impaired proliferation following STING activation in T cells. Although type I IFN facilitates impaired proliferation in T cells in certain conditions (Dickow *et al*, 2019), proliferation impairment following T cell-intrinsic STING activation occurs independently of auto- and paracrine type I interferon signaling. Surprisingly, IRF3 was also dispensable for the antiproliferative effect of STING. Previous studies identified a distinct STING domain within its C-terminal tail (termed "miniCTT") that mediates inhibition of T cell proliferation independent of TBK1 or IRF3 binding (Cerboni *et al*, 2017). In human monocytes, STING-TBK1 has been shown to promote autophosphorylation of ATM, which led to G1 cell cycle arrest through the CHK2-p53-p21 pathway independent of IRF3 (Banerjee *et al*, 2021). It is conceivable that this pathway is also involved in the impairment of cell proliferation in human T cells.

During differentiation following TCR stimulation, T cells undergo metabolic reprogramming to meet bioenergetic demands required for rapid proliferation and differentiation into effector cells, which includes increased uptake of glucose and increased glycolysis. After activation, metabolic reprogramming of T cells is orchestrated by multiple signaling pathways downstream of TCR stimulation, with a prominent role in the PI3K-AKT-mTOR pathway (van der Windt & Pearce, 2012; Le Bourgeois *et al*, 2018). In line with impaired proliferation after TCR stimulation, we also observed a drastic decrease in the ability of T cells to perform glycolysis upon STING activation. Consistent with this observation, STING activation in murine T cells inhibited the assembly of mTORC1, a protein complex that is part of the PI3K-AKT-mTOR pathway involved with metabolic reprogramming (Imanishi *et al*, 2019). Interestingly, STING activation also impaired mitochondrial respiration, which besides the initial phase after activation is characteristic mainly to quiescent T cells (i.e., naïve and memory T cells), which rely on oxidative phosphorylation, glutaminolysis, and fatty acid oxidation (Pearce, 2010). While our model more closely represents TCR-induced proliferation and differentiation into effector cells, decreased mitochondrial respiration upon STING activation further suggests impaired metabolism also in naïve and memory T cells.

Physiological function of STING in T cells

The fact that T cell-intrinsic STING signaling widely impacts T cell functionality raises the question what physiological purpose STING activation in T cells serves. We show that human T cells are capable of canonical STING pathway activation resulting in potent antiviral cytokine release and ISG induction, which opens up the possibility of STING directly sensing infections with T cell tropic viruses. Double-stranded DNA viruses HHV6A, HHV6B, and HHV7 of the betaherpesviridae family predominantly infect CD4 T cells leading to roseola fever initially and often lifelong latency afterwards. It is conceivable that during viral replication in T cells, antiviral factors initiated by cGAS sensing viral DNA are contributing to an antiviral immune response. However, HHV6/7 infection does not induce a type I interferon response (Wang & Pellett, 2007), possibly by viral proteins inhibiting IRF3 (Jaworska *et al*, 2007) as a countermeasure for the detection through a PRR system such as the cGAS-STING pathway.

Considering the substantial effect on T cell function through induction of apoptosis, as well as impaired proliferation and metabolism, cGAS-STING signaling in T cells may also serve as a "safeguard" mechanism following activation and prolonged proliferation as these processes pose a risk for malignancy through the accumulation of DNA damage. cGAS-STING signaling might then be particularly relevant for T cells given their vast proliferative capacity once activated. There is increasing evidence that cGAS-STING senses cytosolic genomic DNA that forms during prolonged TCR stimulation (Li *et al*, 2020; Concepcion *et al*, 2022). As such, cGAS-STING may sense extranuclear DNA, which forms following DNA damage during clonal expansion. Moreover, mitochondrial stress and subsequent mtDNA release were shown to activate cGAS-STING signaling, which we extend to human T cells in this study (Rongvaux *et al*, 2014; White *et al*, 2014; West *et al*, 2015; Wu *et al*, 2019b).

To capitalize on the enhanced immune response against tumor cells after intratumoral STING activation as a therapeutic concept, the application of synthetic, exogenous STING agonists is currently being investigated. While preclinical studies have provided promising results (Corrales *et al*, 2015), subsequent clinical trials have seen mixed results in terms of efficacy (Le Naour *et al*, 2020). This may be due, in part, to reduced functionality of tumor-infiltrating effector T cells following T cell-intrinsic STING activation. In studies with murine tumor models, high dosing regimens of a STING agonist indeed compromised durable tumor control by adaptive immune cells (Sivick *et al*, 2018). Adoptive transfer of STING-deficient T cells in combination with STING agonist treatment could potentially overcome this hurdle and represents a promising new concept for exploiting intratumoral STING activation.

In summary, our study highlights that T cells can indeed contribute to immediate antiviral defenses by producing large amounts of type I interferons in response to cGAS-STING activation. The flip side of the coin is a significant inhibition of T cell function. These distinct roles of STING in human T cells should be considered when this signaling pathway is targeted for immunotherapy.

Materials and Methods

Isolation and culture of human T cells

Peripheral blood mononuclear cells (PBMCs) were isolated from leukocyte reduction system chambers leftover from thrombocyte donation by healthy donors. Approval by the responsible ethics committee and informed consent from all donors according to the declaration of Helsinki were obtained (Project number: 19-238, ethics committee of the Medical Faculty at Ludwig-Maximilians-Universität in Munich). Due to privacy constraints, no information on age, sex, gender, or ethnicity is available for the study participants. Following 1:8 dilution in saline solution, the blood-saline mixture was separated through density gradient centrifugation (Biocoll, Merck #L6115) at 800 *g* for 15 min. PBMCs at the interphase

were collected, diluted 1:2 with PBS and centrifugated (450 *g*, 7 min) for removal of Biocoll. Residual erythrocytes in PBMC pellet were lysed (RBC erythrocyte lysis buffer, Biolegend, #420301) for 5 min on ice. PBMCs were then resuspended in MACS buffer for subsequent negative selection magnetic bead isolation following the manufacturer's instructions (CD4, naïve CD4 and CD8 T cell isolation kit, human; all Miltenyi; #130-096-533, #130-094-131 and #130-096-495, respectively). Sufficient purity following isolation (> 90%) was confirmed by flow cytometry (Fig EV4D).

Cells were then cultured in RPMI 1640 (Thermo Fisher Scientific, #21875-034) supplemented with 10% (v/v) FCS (Gibco, #10270106), 1 mM sodium pyruvate (Gibco, #11360070), 10 mM HEPES (Sigma-Aldrich, #H0887-100ML) and 100 IU/ml penicillin–streptomycin (Thermo Fisher Scientific, #15140163). Additionally, the medium contained 5 ng/ml human recombinant IL7 and IL15 (both Peprotech, #200-07-50ug and #200-15-50ug, respectively).

If not otherwise indicated, 2×10^6 cells were transferred to a 24-well plate coated with 10 µg/ml CD3 (BioLegend, #300438) and 5 µg/ml CD28 (BioLegend, #302902) (incubated in 200 µl PBS at 37°C for 1–2 h, then washed thrice with PBS). Cells were transferred to a new well after 2 days and resupplied once with medium with 50 IU/ml IL2 (R&D Systems, #202-IL-500). Every 2–3 days, cells were resupplied with fresh medium containing IL7 and IL15 keeping a concentration of 0.5–1 $\times 10^6$ cells/ml.

CRISPR/Cas9 knockout in primary human T cells

Polyclonal and clonal CRISPR/Cas9 T cell knockouts were generated as described previously (Linder *et al*, 2020). Briefly, RNPs were produced by mixing synthesized, chemically stabilized tracr- and crRNA (both IDT; 100 pmol each), annealing them at 95°C for 5 min, then letting them cool at room temperature for 30 min. tcr:crRNA pairs were then incubated with 40 pmol of recombinant S.p. NLS-Cas9 (MPI of Biochemistry, Martinsried) for 15 min at room temperature. For the double and triple targeting approach, amounts of tcrRNA and Cas9 were scaled up 2 or 3×. In the case of IRF3, a single gRNA consisting of a fused tcrRNA and crRNA was used, so the annealing step was omitted. 1–2 $\times 10^6$ cells were washed once in PBS, then resuspended in 20 µl P3 buffer (Lonza, #V4XP-3012), mixed with RNPs, and transferred to a 16-well nucleofection plate (Lonza). Cells were then electroporated using the X-unit of a 4D nucleofector (Lonza, program EH100; Seki & Rutz, 2018). After electroporation, cells were transferred to a 24-well plate coated with 10 µg/ml CD3 and 5 µg/ml CD28 in 250 µl RPMI 1640 medium without supplements. After 30–60 min, 250 µl of 2× RPMI 1640 medium with double the supplements and cytokines were added. Cells were then expanded as described above. After 14 days T cells were analyzed for KO efficiency by immunoblotting or Sanger sequencing before being subjected to analysis.

For the generation of single-cell clones with all-allelic knockout for the gene of interest, T cells were subjected to minimal dilution cloning on day 2 of activation in round-bottom 96-well plates. For these experiments, MACS-purified naïve CD4 T cells were cultivated in RPMI supplemented with 2.5% human serum (AB, Sigma-Aldrich, #H5667) containing 50 IU/ml IL2. Monoclones were restimulated on day 8 by the addition of 2,000 αCD3/CD28 beads/well. When colonies became visible after approximately 3 weeks, clones were collected and subjected to MiSeq analysis as described before (Schmid-Burgk *et al*, 2014). In order to obtain sufficient cellular material, all clones generated that were all-allelic knockouts for a certain gene or wildtype were pooled. Wildtype clones from the same donor were pooled from different genome-targeting approaches. For the generation of knockout clones only individual gRNAs were used for STING (gRNA1) and IFNAR1 (gRNA1).

The following gRNAs were used in this study: cGAS gRNA1: CAAAACCGCCCGGAGCTTCG; cGAS gRNA2: CGCATCCCTCCGTACGAGAA; STING gRNA1: GCTGGGACTGCTGTTAAACG; STING gRNA2: GACACGGGATGGATGGATGC; IRF3 sgRNA: GAGGTGACAGCCTTCTACCG; IFNAR1 gRNA1: GCGGCTGCGGACAACACCCA; IFNAR1 gRNA2: GACCCTAGTGCTCGTCGCCG; IFNAR1 gRNA3: GGACAACACCCATGGCGCCA.

Stimulation

Cells were plated at 3 $\times 10^6$ cells/ml in a 24-well plate (500 µl) for western blotting and at 1.33 $\times 10^6$ cells/ml in a 96-well plate (150 µl) for ELISA and flow cytometry. Stimuli were used at the following concentrations, if not indicated otherwise: 20 µg/ml 2′-3′-cGAMP (synthesized in-house, detailed synthesis instructions available upon request) for ELISA and WB, and 40 µg/ml 2′-3′-cGAMP for flow cytometry; 5:1 cells:beads αCD3/CD28 (Gibco, #11132D), 1 µM ABT737 (Selleck Chemicals, #S1002), 1 µM S63845 (Selleck Chemicals, #S8383), 6,000 IU/ml IFNα2a (Miltenyi Biotec, #130-093-874), 20 µM zVAD (R&D Systems, #FMK001), 2 µg/ml PHA (Sigma-Aldrich, #61764), 50 ng/ml PMA (Enzo Life Sciences, #BML-PE160-0005), 1 IU/ml ionomycin (Alomone Labs, #I-700), 10 ng/ml IFNγ (PeproTech, #300-02), 10 ng/ml TNFα (PeproTech, #300-01A), 50 IU/ml IL2 (R&D Systems, #202-IL-010), TPCA-1 (R&D Systems, #2559/10), Dasatinib (Selleck Chemicals, #S1021), Tacrolimus (Astellas Pharma, #06896463), Torin1 (InvivoGen, #inh-tor1), and 2 µM Thapsigargin (Sigma-Aldrich, #T9033-.5MG). For HT-DNA delivery, 200 ng of HT-DNA (Sigma-Aldrich, #D6898-1G) per condition was complexed with 0.5 µl of Lipofectamine 2000 (Thermo Fisher Scientific, #11668019) per condition in Opti-MeM (Gibco, #10149832) for 5 min at RT.

Immunoblotting

After 4 h (if not indicated otherwise) of stimulation, cells were collected from wells, washed once in cold PBS, and lysed in 30 µl DISC buffer containing protease inhibitor (Roche, #11697498001). Samples were spun clear at 18,000 *g* for 10 min. To adjust the protein amount between lanes, protein concentration was measured using a BCA assay (Thermo Fisher Scientific, #23227). Protein was denatured by adding 6× Laemmli buffer and incubating at 78°C for 10 min before freezing samples at −20°C. Supernatants were precipitated with methanol/chloroform in a ratio of 1:1:0.25, resuspended in 1× Laemmli sample buffer, and denatured at 95°C for 10 min (Jakobs *et al*, 2013). Twenty microgram of protein for each sample was separated based on molecular weight through SDS–polyacrylamide gel electrophoresis (Thermo Fisher Scientific, #XP00125BOX) at 120 V for 75 min, then blotted on 0.45 µm nitrocellulose membranes (Amersham Protran, #10600002) at 360 A for 60 min. Membranes were blocked in TBS-T with 3% BSA (Sigma-Aldrich, #A7906-100G) for 15 min, incubated with the indicated primary antibody overnight at 4°C, washed thrice in TBS-T, incubated with

corresponding HRP-linked secondary antibody for 2 h at RT, and washed again. Chemiluminescence was recorded on a Fusion Fx (Vilber) with a CCD camera directly after adding HRP substrate (Millipore, #WBLUF0500). Contrast was enhanced in a linear fashion. The following antibodies were used at 1:1,000 dilution in 3% BSA or 3% milk (for HRP-coupled antibodies): Anti-mouse IgG, HRP-linked (Cell Signaling Technology, #7076P2); Anti-rabbit IgG, HRP-linked (Cell Signaling Technology, #7074S); Human b-Actin-Ab., monoclonal, HRP-conjugated (Santa Cruz, #sc-47778); STING (D2P2F) Rabbit mAb (Cell Signaling Technology, #13647); Phospho-STING (Ser366) (D7C3S) Rabbit mAb (Cell Signaling Technology, #19781); IRF3 (D83B9) Rabbit mAb (Cell Signaling Technology, #4302S); Phospho-IRF-3 (Ser396) (4D4G) Rabbit mAb (Cell Signaling Technology, #4947); Stat1 (9H2) Mouse mAb (Cell Signaling Technology, #9176S); pSTAT1 (Y701) Antibody (Cell Signaling Technology, #7649S), cGAS (D1D3G) Rabbit mAb (Cell Signaling Technology, #15102S), PARP (46D11) Rabbit mAb (Cell Signaling Technology, #9532S), TBK1 (Cell Signaling Technology #3013S), Phospho-TBK1/NAK (Ser172) (D52C2) XP® Rabbit mAb (Cell Signaling Technology, #5483S), Phospho-NF-κB p65 (Ser536) (93H1) Rabbit mAb (Cell Signaling Technology, #3033S), Phospho-IκBα (Ser32) (14D4) Rabbit mAb (Cell Signaling Technology, #2859S), Caspase-3 Antibody (Cell Signaling Technology, #9662S).

Enzyme-linked immunosorbent assay (ELISA) and CellTiter-Glo assay

Supernatant was collected after 48 h of stimulation and frozen at −20°C until analysis. Human IFNβ ELISA, IFNγ ELISA, IFNα ELISA (all R&D Systems, #DY814-05, #DY285B, and #DFNAS0, respectively), and IP10 ELISA (BD Bioscience, #550926) was performed according to the manufacturer's instructions. CellTiter-Glo 2.0 Assay (Promega, #G9243) was performed with residual cells after supernatant removal according to the manufacturer's instructions.

Cell death assay

After 48 h of stimulation, cells were collected, washed once in PBS, and stained with Annexin V (1:40; BioLegend, #640918) in Annexin binding buffer for 15 min at RT. Cells were washed twice in Annexin binding buffer, resuspended in 100 µl buffer containing propidium iodide (1:40; eBioscience, #00-6990-50), and analyzed on a BDFortessa cytometer. Analysis was done in FlowJo. Contour plots (5% levels without outliers) show single events without subcellular debris (see Fig EV4E for gating strategy). Treatment-induced cell death was calculated as (%Annexin V^+PI^+ cells with treatment − %Annexin V^+PI^+ cells without treatment)/(100 − % Annexin V^+PI^+ cells without treatment).

Proliferation assay

Cultured T cells were counted, spun down, and resuspended in CellTrace Violet staining solution (1:1,000 in PBS, Invitrogen, #C34571) in 1 ml per 10^6 cells. Staining solution was incubated at 37°C for 20 min, then quenched with prewarmed cell-culture medium (5× volume of staining solution). Cells were then spun down and plated. Four days later, cells were collected, washed once in PBS, and stained with LIVE/DEAD™ Fixable Near-IR (1:1,000 in PBS; Thermo Fisher Scientific, #L10119) in 50 µl for 20 min at RT in the dark. Cells were washed again in FACS buffer (2% FCS (v/v) PBS + 2 mM EDTA), then stained with anti-CD25 antibody (1:40 in FACS buffer; BioLegend, #356106) in 50 µl for 30 min on ice in the dark. Before analysis on a BDFortessa cytometer (see Fig EV4F for gating strategy), cells were washed twice with FACS buffer. For quantification, individual generations for each peak were calculated using a computer-generated model fitted to the CTV profile by FlowJo. Then, the estimated total number of divisions was divided by the estimated total number of cells, resulting in the division index. Division indices of treated samples were normalized to the nontreated controls by calculating the log2-transformed fold change (log2FC).

Low-input RNA-Seq library preparation and analysis

Following stimulation, 5×10^4 cells per sample were washed lysed with RLT lysis buffer containing 0.04 M DTT and 1% Triton ×100 before storing at −80°C for at least 1 day. Samples were digested with 20 mg/ml Proteinase K for 10 min at 50°C, followed by heat inactivation at 80°C for 10 min. Subsequent RNA/DNA extraction was done by automatic pipetting (Biomek i7, Beckman-Coulter) using RNAdvance Viral Reagent Kit (Beckman-Coulter, #C63510), following the manufacturer's instructions. DNA was digested by incubation with DNAse I for 10 min at 37°C, before adding EDTA (5 mM final concentration) and heat inactivation at 70°C for 10 min. For reverse transcription, RNA barcoding, and library preparation, a modified SCRB-seq protocol (preprint: Soumillon *et al*, 2014) was followed. Samples were sequenced at NGS Core Facility (MPI of Biochemistry, Martinsried) using a NextSeq 500 (Illumina). FASTQC (Andrews, 2010) was used for initial quality control. FASTQ demultiplexing, QC, mapping, and gene counting were done with zUMIs (Parekh *et al*, 2018), and human genome GRCh38 (Howe *et al*, 2020) was used as the reference. All the postmapping analysis and visualization were conducted in R unless specifically stated otherwise. Normalization, exploratory analysis, and differential expression analysis were performed using DESeq2 (Love *et al*, 2014). ggplot2 and ComplexHeatmap were used to visualize the results. Scripts are available upon request. Normalized, filtered read counts and log2-transformed, normalized read counts are available as Datasets EV1 and EV2, respectively.

Glycolysis and mito stress assay

Freshly isolated T cells were activated with αCD3/28 beads for 48 h in the presence or absence of 40 µg/ml cGAMP. Meanwhile, a 96-well Seahorse utility plate (Agilent, #102416-100) was coated 1 day prior to analysis with 18 µl poly-D-lysine at RT for 45 min, washed twice with ddH2O, and dried. A Seahorse sensor cartridge (Agilent, #102416-100) was filled with 200 µl ddH2O and kept overnight in a CO_2-free incubator at 37°C. After 48 h of incubation, cells were depleted of magnetic beads, counted and 2×10^5 viable cells/well were seeded in the previously coated Seahorse 96-well plate and centrifuged at 300 *g* for 3 min at RT. Cells were then incubated for 45 min at 37°C without CO_2 in respective medium: (i) Mitochondria stress assay medium: XF RPMI medium (Agilent, #103576-100) containing 2 mM glutamine (Agilent, #103579-100), 1 mM sodium pyruvate (Agilent, #103578-100) and 10 mM glucose (Agilent,

103577-100), (ii) Glycolysis stress assay medium: XF RPMI medium (Agilent, #103576-100) containing 2 mM glutamine (Agilent, #103579-100). The components of the Seahorse XF Glycolysis and Cell Mito Stress Test Kits (both Agilent, #103020-100 and #103015-100) were reconstituted at the desired stock concentrations and the final dilutions were prepared: (i) Mitochondria stress test: 1 μM Oligomycin, 1 μM FCCP and 1 μM rotenone/antimycin A, (ii) glycolysis stress test: 10 mM Glucose, 1 μM Oligomycin and 50 mM 2-DG. The ddH2O in the sensor cartridge was exchanged with 200 μl calibrant solution and the assay solutions were loaded into the appropriate ports of the hydrated sensor cartridge. Hoechst dye was loaded to the last port, in order to normalize the results to absolute cell numbers. The Seahorse analyzer (Agilent) was calibrated and the cartridge containing the calibrant was exchanged with the cell-containing plate. Metabolic rate data were normalized to viable cell counts based on Hoechst staining using a Citation 1 (BioTek Instruments).

qPCR

RNA was isolated from 2×10^6 expanded CD4 T cells 4 h after stimulation using the Total RNA Purification Mini Spin Column Kit (Genaxxon Bioscience GmbH, #S5304.0250) according to the manufacturer's protocol. The remaining DNA in the extracted RNA was digested using DNaseI (Thermo Scientific, #EN0521). cDNA synthesis were performed with RevertAid Reverse Transcriptase (Thermo Scientific, #EP0442) with Oligo(dT)18 primers. The synthesized cDNA was cleaned up using solid-phase reversible immobilization magnetic beads (GE Healthcare, #GE45152105050250). For the qPCR reaction, TakyonTM No Rox SYBR® MasterMix dTTP Blue (Eurogentec, #UF-NSMT-B0705) was used with the respective primer pairs. The following qPCR primers were used in this study: *TBP1* (fwd: 5′-CCCGAAACGCCGAATATAATCC-3′, rev: 5′-AATCAG TGCCGTGGTTCGTG-3′), *IFNB1* (fwd: 5′-GGCACAACAGGTAGTAG GCG-3′, rev: 5′-GTGGAGAAGCACAACAGGAGA-3′), *OASL* (fwd: 5′-AGGGTACAGATGGGACATCG-3′, rev: 5′-AAGGGTTCACGATGAGG TTG-3′).

Experimental study design

No sample size calculation was made; the sample size was chosen based on past experience and common practice in the field. Blinding was not required for this study because no subjective analyses were performed that would have been biased by knowledge about the samples studied. Rarely, individual data points were excluded from further analysis when technical errors occurred in the measurement process. Also rarely, datasets were intentionally excluded when the positive control did not show a response.

Statistical methods

Normal distribution of the data has been tested on representative data (e.g., cytokine or LDH measurements) using the Shapiro–Wilk test. Statistical significance was calculated as outlined in the respective figure legends with corrections for multiple testing, if relevant. If multiple comparisons are depicted with one comparison bar, the major tick of the comparison bar indicates the reference data to which the statements regarding the level of significance are made. Data plotting and statistical analysis was performed with GraphPad Prism 9.

Data availability

This study includes no data deposited in external repositories. Critical reagents are available upon reasonable request.

Expanded View for this article is available online.

Acknowledgements
We kindly thank the BioSysM FACS core facility for assistance with flow cytometry, the BioSysM Automation Unit for liquid handling, and Claudia Ludwig (Gene Center, LMU) for great technical support. This study was supported by funding from the Deutsche Forschungsgemeinschaft (DFG, German Research Foundation) SFB TRR 338 (project ID 452881907) to VH, MS, and ST and SFB 1054 (project ID 210592381) to VH. AL is supported by a fellowship of the Else Kröner-Forschungskolleg: Cancer Immunotherapy and the FöFoLe program of the LMU. Open Access funding enabled and organized by Projekt DEAL.

Author contributions
Niklas Kuhl: Conceptualization; investigation; writing – original draft; writing – review and editing. **Andreas Linder:** Conceptualization; investigation; writing – original draft; writing – review and editing. **Nora Philipp:** Investigation. **Daniel Nixdorf:** Investigation. **Hannah Fischer:** Investigation. **Simon Veth:** Investigation. **Gunnar Kuut:** Investigation. **Teng Teng Xu:** Investigation. **Sebastian Theurich:** Resources; supervision; funding acquisition. **Thomas Carell:** Resources; supervision; funding acquisition. **Marion Subklewe:** Resources; supervision; funding acquisition. **Veit Hornung:** Conceptualization; resources; data curation; supervision; funding acquisition; writing – original draft; writing – review and editing.

Disclosure and competing interests statement
The authors declare that they have no conflict of interest.

References

Abe T, Barber GN (2014) Cytosolic-DNA-mediated, STING-dependent proinflammatory gene induction necessitates canonical NF-κB activation through TBK1. *J Virol* 88: 5328 – 5341

Ablasser A, Goldeck M, Cavlar T, Deimling T, Witte G, Röhl I, Hopfner K-P, Ludwig J, Hornung V (2013) cGAS produces a 2′-5′-linked cyclic dinucleotide second messenger that activates STING. *Nature* 498: 380 – 384

Andrews S (2010) FastQC: a quality control tool for high throughput sequence data. https://www.bioinformatics.babraham.ac.uk/projects/fastqc/

Au WC, Moore PA, Lowther W, Juang YT, Pitha PM (1995) Identification of a member of the interferon regulatory factor family that binds to the interferon-stimulated response element and activates expression of interferon-induced genes. *Proc Natl Acad Sci USA* 92: 11657 – 11661

Banerjee D, Langberg K, Abbas S, Odermatt E, Yerramothu P, Volaric M, Reidenbach MA, Krentz KJ, Rubinstein CD, Brautigan DL *et al* (2021) A non-canonical, interferon-independent signaling activity of cGAMP triggers DNA damage response signaling. *Nat Commun* 12: 6207

Benoit-Lizon I, Jacquin E, Rivera Vargas T, Richard C, Roussey A, Dal Zuffo L, Martin T, Melis A, Vinokurova D, Shahoei SH *et al* (2022) CD4 T cell-intrinsic STING signaling controls the differentiation and effector functions of T_H1 and T_H9 cells. *J Immunother Cancer* 10: e003459

Bouis D, Kirstetter P, Arbogast F, Lamon D, Delgado V, Jung S, Ebel C, Jacobs H, Knapp A-M, Jeremiah N *et al* (2019) Severe combined immunodeficiency in stimulator of interferon genes (STING) V154M/wild-type mice. *J Allergy Clin Immunol* 143: 712 – 725

Burdette DL, Monroe KM, Sotelo-Troha K, Iwig JS, Eckert B, Hyodo M, Hayakawa Y, Vance RE (2011) STING is a direct innate immune sensor of cyclic di-GMP. *Nature* 478: 515 – 518

Cerboni S, Jeremiah N, Gentili M, Gehrmann U, Conrad C, Stolzenberg M-C, Picard C, Neven B, Fischer A, Amigorena S *et al* (2017) Intrinsic antiproliferative activity of the innate sensor STING in T lymphocytes. *J Exp Med* 214: 1769 – 1785

Chattopadhyay S, Marques JT, Yamashita M, Peters KL, Smith K, Desai A, Williams BRG, Sen GC (2010) Viral apoptosis is induced by IRF-3-mediated activation of Bax. *EMBO J* 29: 1762 – 1773

Concepcion AR, Wagner LE, Zhu J, Tao AY, Yang J, Khodadadi-Jamayran A, Wang Y-H, Liu M, Rose RE, Jones DR *et al* (2022) The volume-regulated anion channel LRRC8C suppresses T cell function by regulating cyclic dinucleotide transport and STING–p53 signaling. *Nat Immunol* 23: 287 – 302

Corrales L, Glickman LH, McWhirter SM, Kanne DB, Sivick KE, Katibah GE, Woo S-R, Lemmens E, Banda T, Leong JJ *et al* (2015) Direct activation of STING in the tumor microenvironment leads to potent and systemic tumor regression and immunity. *Cell Rep* 11: 1018 – 1030

de Oliveira Mann CC, Orzalli MH, King DS, Kagan JC, Lee ASY, Kranzusch PJ (2019) Modular architecture of the STING C-terminal tail allows interferon and NF-κB signaling adaptation. *Cell Rep* 27: 1165 – 1175

Dickow J, Francois S, Kaiserling R-L, Malyshkina A, Drexler I, Westendorf AM, Lang KS, Santiago ML, Dittmer U, Sutter K (2019) Diverse immunomodulatory effects of individual IFNα subtypes on virus-specific $CD8^+$ T cell responses. *Front Immunol* 10: 2255

Diner EJ, Burdette DL, Wilson SC, Monroe KM, Kellenberger CA, Hyodo M, Hayakawa Y, Hammond MC, Vance RE (2013) The innate immune DNA sensor cGAS produces a noncanonical cyclic dinucleotide that activates human STING. *Cell Rep* 3: 1355 – 1361

Dou Z, Ghosh K, Vizioli MG, Zhu J, Sen P, Wangensteen KJ, Simithy J, Lan Y, Lin Y, Zhou Z *et al* (2017) Cytoplasmic chromatin triggers inflammation in senescence and cancer. *Nature* 550: 402 – 406

Dufva O, Koski J, Maliniemi P, Ianevski A, Klievink J, Leitner J, Pölönen P, Hohtari H, Saeed K, Hannunen T *et al* (2020) Integrated drug profiling and CRISPR screening identify essential pathways for CAR T-cell cytotoxicity. *Blood* 135: 597 – 609

Fang R, Wang C, Jiang Q, Lv M, Gao P, Yu X, Mu P, Zhang R, Bi S, Feng J-M *et al* (2017) NEMO–IKKβ are essential for IRF3 and NF-κB activation in the cGAS–STING pathway. *J Immunol* 199: 3222 – 3233

Gao P, Ascano M, Wu Y, Barchet W, Gaffney Barbara L, Zillinger T, Serganov Artem A, Liu Y, Jones Roger A, Hartmann G *et al* (2013) Cyclic [G(2′,5′)pA(3′,5′)p] is the metazoan second messenger produced by DNA-activated cyclic GMP-AMP synthase. *Cell* 153: 1094 – 1107

Glück S, Guey B, Gulen MF, Wolter K, Kang T-W, Schmacke Niklas A, Bridgeman A, Rehwinkel J, Zender L, Ablasser A (2017) Innate immune sensing of cytosolic chromatin fragments through cGAS promotes senescence. *Nat Cell Biol* 19: 1061 – 1070

Green DR, Droin N, Pinkoski M (2003) Activation-induced cell death in T cells. *Immunol Rev* 193: 70 – 81

Gulen MF, Koch U, Haag SM, Schuler F, Apetoh L, Villunger A, Radtke F, Ablasser A (2017) Signalling strength determines proapoptotic functions of STING. *Nat Commun* 8: 427

Harding SM, Benci JL, Irianto J, Discher DE, Minn AJ, Greenberg RA (2017) Mitotic progression following DNA damage enables pattern recognition within micronuclei. *Nature* 548: 466 – 470

Honda K, Takaoka A, Taniguchi T (2006) Type I inteferon gene induction by the interferon regulatory factor family of transcription factors. *Immunity* 25: 349 – 360

Howe KL, Contreras-Moreira B, De Silva N, Maslen G, Akanni W, Allen J, Alvarez-Jarreta J, Barba M, Bolser DM, Cambell L *et al* (2020) Ensembl Genomes 2020-enabling non-vertebrate genomic research. *Nucleic Acids Res* 48: D689 – D695

Imanishi T, Unno M, Kobayashi W, Yoneda N, Matsuda S, Ikeda K, Hoshii T, Hirao A, Miyake K, Barber GN *et al* (2019) Reciprocal regulation of STING and TCR signaling by mTORC1 for T-cell activation and function. *Life Sci Alliance* 2: e201800282

Ishikawa H, Barber GN (2008) STING is an endoplasmic reticulum adaptor that facilitates innate immune signalling. *Nature* 455: 674 – 678

Iwanaszko M, Kimmel M (2015) NF-κB and IRF pathways: cross-regulation on target genes promoter level. *BMC Genomics* 16: 307

Jakobs C, Bartok E, Kubarenko A, Bauernfeind F, Hornung V (2013) Immunoblotting for active caspase-1. *Methods Mol Biol* 1040: 103 – 115

Jaworska J, Gravel A, Fink K, Grandvaux N, Flamand L (2007) Inhibition of transcription of the beta interferon gene by the human herpesvirus 6 immediate-early 1 protein. *J Virol* 81: 5737 – 5748

Larkin B, Ilyukha V, Sorokin M, Buzdin A, Vannier E, Poltorak A (2017) Cutting edge: activation of STING in T cells induces type I IFN responses and cell death. *J Immunol* 199: 397 – 402

Le Bourgeois T, Strauss L, Aksoylar H-I, Daneshmandi S, Seth P, Patsoukis N, Boussiotis VA (2018) Targeting T cell metabolism for improvement of cancer immunotherapy. *Front Oncol* 8: 237

Le Naour J, Zitvogel L, Galluzzi L, Vacchelli E, Kroemer G (2020) Trial watch: STING agonists in cancer therapy. *Oncoimmunology* 9: 1777624

Li T, Chen ZJ (2018) The cGAS–cGAMP–STING pathway connects DNA damage to inflammation, senescence, and cancer. *J Exp Med* 215: 1287 – 1299

Li W, Lu L, Lu J, Wang X, Yang C, Jin J, Wu L, Hong X, Li F, Cao D *et al* (2020) cGAS-STING–mediated DNA sensing maintains $CD8^+$ T cell stemness and promotes antitumor T cell therapy. *Sci Transl Med* 12: eaay9013

Lin R, Heylbroeck C, Pitha PM, Hiscott J (1998) Virus-dependent phosphorylation of the IRF-3 transcription factor regulates nuclear translocation, transactivation potential, and proteasome-mediated degradation. *Mol Cell Biol* 18: 2986 – 2996

Linder A, Bauernfried S, Cheng Y, Albanese M, Jung C, Keppler OT, Hornung V (2020) CARD8 inflammasome activation triggers pyroptosis in human T cells. *EMBO J* 39: e105071

Love MI, Huber W, Anders S (2014) Moderated estimation of fold change and dispersion for RNA-seq data with DESeq2. *Genome Biol* 15: 550

Mackenzie KJ, Carroll P, Martin C-A, Murina O, Fluteau A, Simpson DJ, Olova N, Sutcliffe H, Rainger JK, Leitch A *et al* (2017) cGAS surveillance of micronuclei links genome instability to innate immunity. *Nature* 548: 461 – 465

Ning X, Wang Y, Jing M, Sha M, Lv M, Gao P, Zhang R, Huang X, Feng J-M, Jiang Z (2019) Apoptotic caspases suppress type I interferon production via the cleavage of cGAS, MAVS, and IRF3. *Mol Cell* 74: 19 – 31

Parekh S, Ziegenhain C, Vieth B, Enard W, Hellmann I (2018) zUMIs - a fast and flexible pipeline to process RNA sequencing data with UMIs. *Gigascience* 7: giy059

Pearce EL (2010) Metabolism in T cell activation and differentiation. *Curr Opin Immunol* 22: 314 – 320

Rongvaux A, Jackson R, Harman Christian CD, Li T, West AP, de Zoete Marcel R, Wu Y, Yordy B, Lakhani Saquib A, Kuan C-Y *et al* (2014) Apoptotic caspases prevent the induction of type I interferons by mitochondrial DNA. *Cell* 159: 1563 – 1577

Samarajiwa SA, Forster S, Auchettl K, Hertzog PJ (2009) INTERFEROME: the database of interferon regulated genes. *Nucleic Acids Res* 37: D852 – D857

Schmid-Burgk JL, Schmidt T, Gaidt MM, Pelka K, Latz E, Ebert TS, Hornung V (2014) OutKnocker: a web tool for rapid and simple genotyping of designer nuclease edited cell lines. *Genome Res* 24: 1719 – 1723

Seki A, Rutz S (2018) Optimized RNP transfection for highly efficient CRISPR/Cas9-mediated gene knockout in primary T cells. *J Exp Med* 215: 985 – 997

Sivick KE, Desbien AL, Glickman LH, Reiner GL, Corrales L, Surh NH, Hudson TE, Vu UT, Francica BJ, Banda T *et al* (2018) Magnitude of therapeutic STING activation determines $CD8^+$ T cell-mediated anti-tumor immunity. *Cell Rep* 25: 3074 – 3085

Soboloff J, Rothberg BS, Madesh M, Gill DL (2012) STIM proteins: dynamic calcium signal transducers. *Nat Rev Mol Cell Biol* 13: 549 – 565

Soumillon M, Cacchiarelli D, Semrau S, Oudenaarden AV, Mikkelsen TS (2014) Characterization of directed differentiation by high-throughput single-cell RNA-Seq. *bioRxiv* https://doi.org/10.1101/003236 [PREPRINT]

Srikanth S, Woo JS, Wu B, El-Sherbiny YM, Leung J, Chupradit K, Rice L, Seo GJ, Calmettes G, Ramakrishna C *et al* (2019) The Ca^{2+} sensor STIM1 regulates the type I interferon response by retaining the signaling adaptor STING at the endoplasmic reticulum. *Nat Immunol* 20: 152 – 162

Sun L, Wu J, Du F, Chen X, Chen ZJ (2013) Cyclic GMP-AMP synthase is a cytosolic DNA sensor that activates the type I interferon pathway. *Science* 339: 786 – 791

van der Windt GJW, Pearce EL (2012) Metabolic switching and fuel choice during T-cell differentiation and memory development. *Immunol Rev* 249: 27 – 42

Wang F-Z, Pellett PE (2007) HHV-6A, 6B, and 7: immunobiology and host response. In *Human Herpesviruses: Biology, Therapy, and Immunoprophylaxis*, Arvin A, Campadelli-Fiume G, Mocarski E, Moore PS, Roizman B, Whitley R, Yamanishi K (eds). Cambridge: Cambridge University Press

Warner JD, Irizarry-Caro RA, Bennion BG, Ai TL, Smith AM, Miner CA, Sakai T, Gonugunta VK, Wu J, Platt DJ *et al* (2017) STING-associated vasculopathy develops independently of IRF3 in mice. *J Exp Med* 214: 3279 – 3292

West AP, Khoury-Hanold W, Staron M, Tal MC, Pineda CM, Lang SM, Bestwick M, Duguay BA, Raimundo N, MacDuff DA *et al* (2015) Mitochondrial DNA stress primes the antiviral innate immune response. *Nature* 520: 553 – 557

White MJ, McArthur K, Metcalf D, Lane RM, Cambier JC, Herold MJ, van Delft MF, Bedoui S, Lessene G, Ritchie ME *et al* (2014) Apoptotic caspases suppress mtDNA-induced STING-mediated type I IFN production. *Cell* 159: 1549 – 1562

Wu J, Chen Y-J, Dobbs N, Sakai T, Liou J, Miner JJ, Yan N (2019a) STING-mediated disruption of calcium homeostasis chronically activates ER stress and primes T cell death. *J Exp Med* 216: 867 – 883

Wu Z, Oeck S, West AP, Mangalhara KC, Sainz AG, Newman LE, Zhang X-O, Wu L, Yan Q, Bosenberg M *et al* (2019b) Mitochondrial DNA stress signalling protects the nuclear genome. *Nat Metab* 1: 1209 – 1218

Wu J, Dobbs N, Yang K, Yan N (2020) Interferon-independent activities of mammalian STING mediate antiviral response and tumor immune evasion. *Immunity* 53: 115 – 126

Yang H, Wang H, Ren J, Chen Q, Chen ZJ (2017) cGAS is essential for cellular senescence. *Proc Natl Acad Sci USA* 114: E4612 – E4620

Zhang X, Shi H, Wu J, Zhang X, Sun L, Chen C, Chen ZJ (2013) Cyclic GMP-AMP containing mixed phosphodiester linkages is an endogenous high-affinity ligand for STING. *Mol Cell* 51: 226 – 235